RESEARCH ARTICLE

CrossMark

Emplacement of the Rocche Rosse rhyolite lava flow (Lipari, Aeolian Islands)

Liam A. Bullock[1,2] · Ralf Gertisser[1] · Brian O'Driscoll[1,3]

Abstract

The Rocche Rosse lava flow marks the most recent rhyolitic extrusion on Lipari island (Italy), and preserves evidence for a multi-stage emplacement history. Due to the viscous nature of the advancing lava (10^8 to 10^{10} Pa s), indicators of complex emplacement processes are preserved in the final flow. This study focuses on structural mapping of the flow to highlight the interplay of cooling, crust formation and underlying slope in the development of rhyolitic lavas. The flow is made up of two prominent lobes, small (< 0.2 m) to large (> 0.2 m) scale folding and a channelled geometry. Foliations dip at 2–4° over the flatter topography close to the vent, and up to 30–50° over steeper mid-flow topography. Brittle faults, tension gashes and conjugate fractures are also evident across flow. Heterogeneous deformation is evident through increasing fold asymmetry from the vent due to downflow cooling and stagnation. A steeper underlying topography mid-flow led to development of a channelled morphology, and compression at topographic breaks resulted in fold superimposition in the channel. We propose an emplacement history that involved the evolution through five stages, each associated with the following flow regimes: (1) initial extrusion, crustal development and small scale folding; (2) extensional strain, stretching lineations and channel development over steeper topography; (3) compression at topographic break, autobrecciation, lobe development and medium scale folding; (4) progressive deformation with stagnation, large-scale folding and refolding; and (5) brittle deformation following flow termination. The complex array of structural elements observed within the Rocche Rosse lava flow facilitates comparisons to be made with actively deforming rhyolitic lava flows at the Chilean volcanoes of Chaitén and Cordón Caulle, offering a fluid dynamic and structural framework within which to evaluate our data.

Keywords Rhyolite · Blocky lava flow · Folds · High viscosity · Deformation · Obsidian

---

✉ Liam A. Bullock
liam.bullock@abdn.ac.uk

1 School of Geography, Geology and the Environment, Keele University, Keele, Staffordshire ST5 5BG, UK

2 Department of Geology and Petroleum Geology, University of Aberdeen, King's College, Meston Building, Aberdeen AB24 3UE, UK

3 School of Earth and Environmental Sciences, University of Manchester, Williamson Building, Oxford Road, Manchester M13 9PL, UK

Introduction

While the structural emplacement of basaltic lava flows is well-constrained (e.g. Pinkerton and Sparks 1978; Lipman and Banks 1987; Self et al. 1997; Calvari and Pinkerton 1999; Cashman et al. 1999; Kilburn 2000; Jerram 2002, Passey and Bell 2007), such studies of more silicic lava flows are comparatively few (e.g. Fink 1983; de Silva et al. 1994; Fujii and Nakada 1999; Uia et al. 1999; Castro et al. 2002; Harris et al. 2002; Cioni and Funedda 2005; Tuffen et al. 2013; Magnall et al. 2016, 2017; Latutrie et al. 2017). This is due in part to a lack of observations of active flows. Prior to 2008, no rhyolite-forming eruption had been witnessed and documented (Tuffen et al. 2013; Schipper et al. 2013; Castro et al. 2014). As a result of this, our understanding of the mechanics of basaltic lava flow emplacement is confirmed by real-time observations, while our knowledge of rhyolitic lava

🌍 Springer

flow emplacement has generally been inferred based on the structural configuration of preserved flows (e.g. Fink 1983; Manga 1998; Tuffen et al. 2013; Magnall et al. 2016).

The Rocche Rosse rhyolite lava flow on the island of Lipari (Aeolian Islands, Italy; Fig. 1) shows exceptional preservation of complex small to large-scale structures. Previous work on the Rocche Rosse has focused on fragmentation and transport mechanisms of the associated pyroclastic sequence (Dellino and La Volpe 1995), the thermal history of flow frontal ramps, i.e. ridges of fold structures extending downward into the flow by tens of metres (Gottsmann and Dingwell 2001), magmatic history (Gioncada et al. 2003, 2005; Davì et al. 2009, 2010) and textural heterogeneity (Gonnermann and Manga 2003; Clay et al. 2013; Shields et al. 2016). Ramp structures of the Rocche Rosse were also documented by Hall (1978) and Cas and Wright (1987), inferring a compressive regime and build-up of lava behind a brecciated flow front, hindering flow advance. Well-exposed surface and flank structures resulted from surface crust development, and sequential emplacement and deformation history. Such structures are often evident and have been studied in viscous intermediate lava flows (e.g. Cerro Chao, Chile—Fink 1980b; de Silva et al. 1994; Puy de Cliergue, France—Latutrie et al. 2017; San Pietro, Sardinia—Cioni and Funedda 2005; Santiaguito, Guatemala—Harris et al. 2002, 2004), and other rhyolitic lava flows worldwide (Fink 1980a, b 1983; Manley and Fink 1987; Carn et al. 2009; Lara 2009; Bernstein et al. 2013; Pallister et al. 2013; Tuffen et al. 2013; Magnall et al. 2017).

Previous studies of rhyolite lava flow crust development and emplacement mechanisms have centred on United States Holocene flows (Big and Little Glass Mountain, Medicine Lake; Fink 1980a, b, 1983; Manley and Fink 1987; Manga 1998; Big Obsidian Flow in Newberry Caldera; Castro et al. 2002). Early conceptual models of rhyolite lava flow emplacement depict slowly spreading lavas overriding blocks of surface crust, creating an upper and basal breccia (Fink 1980a, 1983; Manley and Fink 1987), before stopping when supply has ceased. Processes such as rising pumice diapirs, compression, extension and fracture propagation produce a range of complex surface structural relations (Fink 1983). For instance, the development of a cooled surface crust promotes crustal folding during flow advance (Fink 1980a; Castro and Cashman 1999) and crease structure development (Anderson and Fink 1992; Lescinsky and Merle 2005). Crusts influence lava flow growth (Griffiths and Fink 1992; Fink and Griffiths 1998), and thermally insulate the flow, facilitating prolonged mobility and advance (Swanson 1973; Manley 1992; Fink and Griffiths 1998; Keszthelyi and Self 1998; Harris and Rowland 2009; Tuffen et al. 2013). This has been previously observed in dacitic lava flow emplacement at Santiaguito (Harris et al. 2002, 2004), and active rhyolitic flow emplacement at Puyehue-Cordón Caulle (Tuffen et al. 2013; Magnall et al. 2017).

Since 2008, real-time observations of active rhyolitic flow and dome emplacement at the Chilean volcanoes of Chaitén (Carn et al. 2009; Lara 2009; Bernstein et al. 2013; Pallister et al. 2013) and Puyehue-Cordón Caulle (Castro et al. 2013; Schipper et al. 2013; Tuffen et al. 2013; Bertin et al. 2015; Farquharson et al. 2015; Magnall et al. 2017) have further developed our knowledge of rhyolitic lava emplacement. The Cordón Caulle eruption is an example of a flow that moved away from the vent, while Chaitén was a dome-forming eruption. Observations of the 2008 Chaitén eruption and associated composite rhyolite dome highlight simultaneous explosive and effusive activity, exogenous and endogenous growth phases and complex lava lobe and spine formation (Carn et al. 2009; Lara 2009; Bernstein et al. 2013; Pallister et al. 2013). These resulted from multiple flow paths (flow directions of areas of active dome growth) within the lava dome, and different extrusion rates (Carn et al. 2009; Lara 2009; Bernstein et al. 2013; Pallister et al. 2013). Morphological observations of the 2011–2012 Cordón Caulle eruption highlight the role of thermal insulation by a surface crust in prolonging flow-horizontal transport, channelled flow, surface crust formation, development of breakout lobes and flow frontal stalling (Castro et al. 2013; Schipper et al. 2013; Tuffen et al. 2013; Bertin et al. 2015; Magnall et al. 2017). In these studies, comparisons are made to basaltic lava flow fields, with common controlling mechanisms that work towards a unified model of effusive eruptions (Castro et al. 2013; Schipper et al. 2013; Tuffen et al. 2013; Bertin et al. 2015; Magnall et al. 2017).

While active observations can act as benchmarks for future rhyolite effusive events, they can also improve interpretations of past eruptions. Specifically, morphological features observed in real-time eruptions can help to decipher how structures were formed and modified in older flows. Observations of active rhyolite lava effusion at Chaitén and Cordón Caulle (Carn et al. 2009; Lara 2009; Castro et al. 2013; Tuffen et al. 2013) provide a new motivation to revisit the emplacement mechanisms of older rhyolite lava flows such as the Rocche Rosse flow. This study aims to focus on Rocche Rosse flow morphology, satellite observations and structural measurements, using detailed qualitative and quantitative structural measurements to formulate new interpretations of the flow dynamics associated with emplacement of the Rocche Rosse flow. Surface structures and flank (edge of flow) characteristics are examined to provide further insights into the internal architecture of the Rocche Rosse, and the important role played by progressive deformation and channelled flow morphology in rhyolite lava flow structural evolution.

Geological setting

The Aeolian archipelago (Fig. 1) is the result of the complex collision between the African and Eurasian plates (Ventura 2013). The historically active island of Lipari is located in the centre of the archipelago, and is the largest island (Fig. 1). The NNW-SSE striking Tindari-Letojanni fault system defines the alignment of volcanoes (Barberi et al. 1994, Fig. 1). Re-activation of the fault during the middle- to late-Pleistocene caused recent volcanism in the central arc (Barberi et al. 1994; Gvirtzman and Nur 2001; Ventura 2013). Lipari rises ~600 m above sea level and lies on 20-km-thick continental crust (Finetti and Morelli 1973).

The most recent activity of Lipari comprised explosive pyroclastic deposits and rhyolitic lava flows, culminating in the extrusion of the Rocche Rosse and Forgia Vecchia rhyolite lava flows (Forni et al. 2013). The pattern of this recent activity included a hydromagmatic phase, explosive eruption of a vesicular magma, accompanying fall and surge deposits and degassed viscous lava extrusion (Cortese et al. 1986; Dellino and La Volpe 1995; Lucchi et al. 2010; Forni et al. 2013). The

Rocche Rosse represents a renewal of activity, following the initial Monte Pilato-Rocche Rosse explosive phase. The age of the Rocche Rosse, as determined by archaeomagnetic methods, is 1230 ± 40 AD (Arrighi et al. 2006).

Lithofacies of rhyolitic lava flows

Rhyolitic lava flows show a complex internal sequence with variably vesicular, devitrified and deformed textures, and complex surface deformation patterns (Fink 1978, 1983; Manley and Fink 1987; Shields et al. 2016). The traditional view of rhyolitic flow interiors includes (from the surface downwards) an upper breccia, thick obsidian, foliated rhyolite, thinner obsidian and a basal breccia (Fink 1978, 1983; Manley and Fink 1987). This idealised cross section has been observed in Obsidian Dome core drills in California, the Banco Bonito flow in New Mexico (Manley and Fink 1987) and Little Glass Mountain (Medicine Lake) (Fink 1983). Spherulitic and crystalline lava forms the central part of the flow, with the population density of crystals and spherulites

Fig. 1 **a** The Aeolian Islands, southern Tyrrhenian Sea (Italy), with Lipari in the centre of the archipelago, straddling the Tindari-Letojanni fault system (Ventura 2013), and **b** the Rocche Rosse lava flow in NE Lipari. **c** Google Earth image of the Rocche Rosse (view to the south) (Map data: SOI, NOAA, U.S. Navy, NGA, GEBCO, TerraMetrics, ©2018 Google)
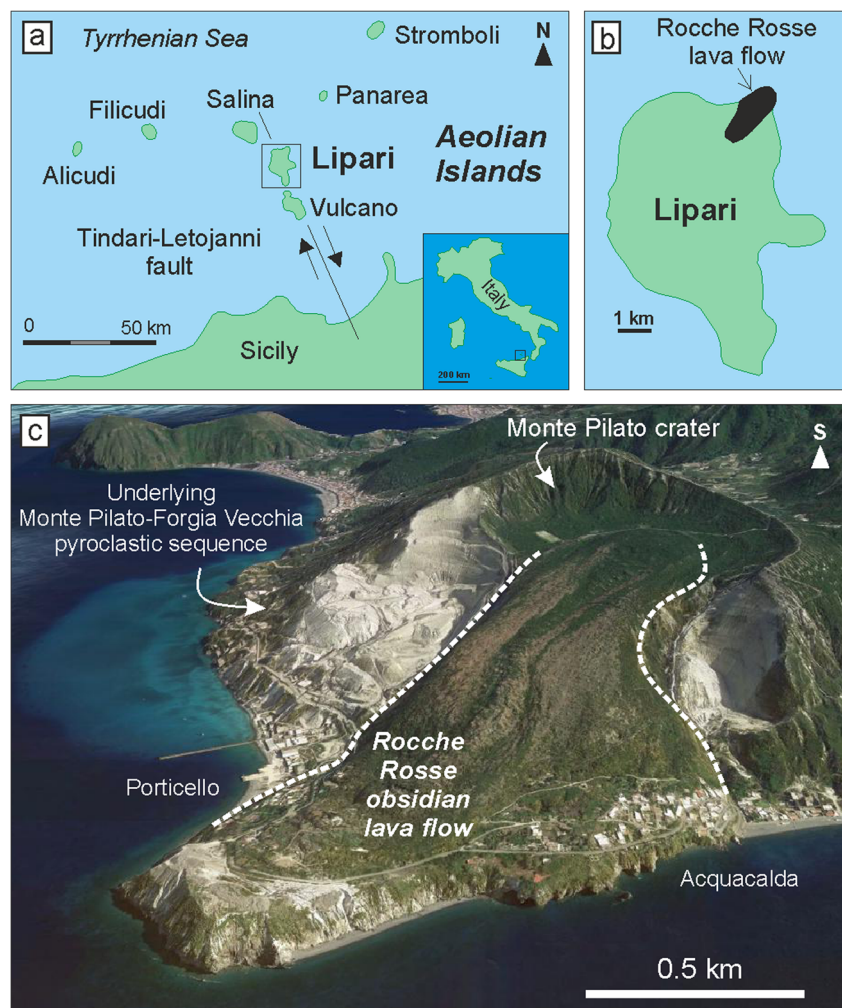
depending on the length and thickness of the flow (Manley and Fink 1987). Spherulites are radial fibrous crystallites, considered to progressively nucleate as a down temperature continuum during syn- and post-emplacement cooling (Lofgren 1971; Swanson 1977; McArthur et al. 1998; Gardner et al. 2012; Breitkreuz 2013; Clay et al. 2013; Bullock et al. 2017). Differences in spherulite abundance (often manifested as trails), crystallinity, vesicularity and glass chemistry can all define flow foliation in rhyolite (Gonnermann and Manga 2005; Clay et al. 2013; Bullock et al. 2017).

The structural arrangement of flow foliations preserves a record of deformation associated with flow emplacement (Gonnermann and Manga 2003; Cioni and Funedda 2005), a record of brittle-ductile processes (Castro et al. 2008) and the analysis of foliation patterns contributes to the understanding of the structural evolution undergone during polyphase deformation of rocks (Fink 1978, 1983; Manley and Fink 1987; Manga 1998; Gonnerman and Manga 2005). The determination of a preferred orientation of foliations (and lineations) can also provide a record of strain, lava flow and deformation. Fink (1983) identified three deformational processes that disrupted the foliation of the flow during advance: (1) low density coarsely vesicular pumice diapirs, which rise and cause surface doming and plunging anticlines; (2) flow-parallel compressional stresses near the flow front, resulting in flow folding oriented transverse to flow direction; and (3) an extensional regime, resulting in inward propagating surface fractures.

Records of flow emplacement and deformation in the Rocche Rosse are recognisable due to textural variations within the flow. Shields et al. (2016) identified four textural units in the Rocche Rosse: type 1—glassy obsidian, which is spherulitic and has a low vesicularity (< 15%); type 2—'frothy' obsidian, which is vesicular (30–60%) and glassy, with large elongated vesicles perpendicular to banding; type 3—pumiceous lava, which is highly vesicular (40–60%), with variable vesicle sizes; type 4—shear banded lava, characterised by a low-medium vesicularity (20–40%), and highly deformed and coalesced vesicles. Glassy obsidian and shear banded lavas occur as massive and/or platy outcrops, pumiceous lava is observed throughout the flow and 'frothy' obsidian makes up fold hinges, tension gashes, micro folding and extensional fractures (Shields et al. 2016).

Textural variations such as glassy and devitrified obsidian as well as vesicular units can be identified at middle- and upper-flow regions, and brecciated zones are evident across the entire flow. Flow stratigraphy is exposed along the flanks of the Rocche Rosse, visible from the town of Acquacalda to the west and Porticello to the east (Fig. 2). The Rocche Rosse sits on top of older tephra deposits (Forni et al. 2013). A thick (up to 10 m) basal breccia made up of angular obsidian blocks is evident at the base of the flow (Fig. 2). Pumiceous lava (grey-white, variable sizes and shapes of vesicles, low density) and obsidian (black, glassy or devitrified, poorly vesicular and high density spherulitic lava) lithofacies sit on top of the basal breccia.

Methodology

In this study, the Rocche Rosse is characterised by mapping based on high spatial resolution satellite imagery, flank/surface observations and structural measurements. Large-scale surface structures were observed and measured from Infoterra GeoEye-1 satellite imagery (obtained from Airbus Defence and Space) at a 0.5 m resolution. The GeoEye-1 image covers an area of 5010 km^2 at a scale of 1:10,000. Large-scale lineaments were identified, traced and measured using *ArcMap 10* geo-referenced measurement tools. Here, 'lineament' is used as a descriptive term for a linear or curvilinear surface feature identified in GeoEye-1 imagery analyses. Measurements of large scale folds were cross-checked with kinematic data collected in the field. The flow stratigraphy and thickness of the Rocche Rosse is visible along the eastern and western flank exposures (Fig. 2). Flow thickness was calculated at various points around the flanks using a comparable scaling technique (comparing with an object of known height, e.g. a 1 m scale bar).

Flow foliation was identified by the planar arrangement of spherulites, microlites and vesicularity. Foliation attitude was recorded and mapped as strike, dip and dip direction. Folds were measured and described based on their fold axial plane (strike and dip) and fold axis (orientation and inclination of hinge-line measured as a lineation). Wavelength and amplitude of folds were also measured. Stretching lineations, evident as a three-dimensional parallel alignment of flattened spherulites, were measured in terms of plunge angle and azimuth. Stereographs, density plots and rose diagrams were created using *Stereo32* software, projected as equal area lower hemisphere plots. Stereoplots were used to graphically represent measured surface structures, with density plots highlighting the density concentrations of data and rose diagrams graphically summarising directional data. All of the data are summarised based on the average agreement of data to the most common orientation. For instance, if foliation measurements were entirely random across flow, we infer that the flow has no degree of preferred orientation. If there is some agreement of the data in a single direction, we infer that the flow shows a weak, moderate or strong degree of orientation. More specifically, no degree of preferred orientation is deemed as being associated with a correlation of less than 20%, a weak degree of preferred orientation is 20–50%, a moderate degree of preferred orientation is 50–70% and a strong degree of preferred orientation is > 70%.
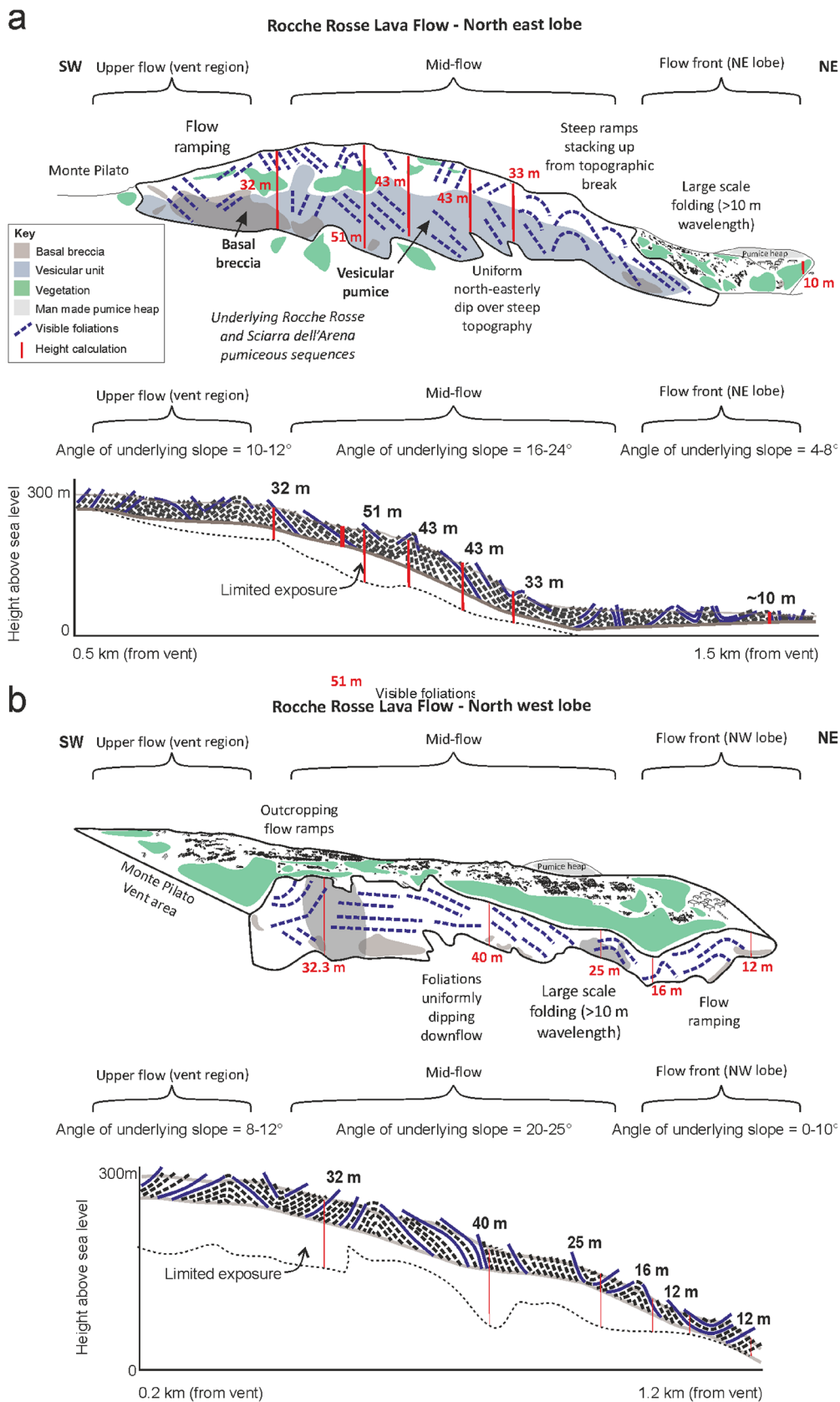
Fig. 2 Digitisation of **a** NE and **b** NW flow flanks and flow divisions. Flow thickness and textural variations shown, as well as dominant observed foliation attitude. General attitude of foliations indicated by dashed lines, vesicular zones shown in grey and basal breccia in brown

Results

Overall flow morphology

Most of the flow surface is exposed, except in flow frontal regions where exposures are restricted by a man-made pumice heap. The flow extends from an elevation of 310 m to sea level. The maximum flow length measured by GeoEye-1 imagery (Fig. 3) is 2060 m, and the maximum width of the flow is 1130 m. There are three key structural features evident (Fig. 3): (1) lineaments aligned roughly SW-NE, sub-parallel to flow direction from the Monte Pilato vent to the SW, (2) curvilinear features roughly parallel to the flow front and (3) two prominent flow-front headlands. Lineaments extend from near-vent to mid-flow regions (extending over tens to hundreds of metres). Less prominent, smaller scale lineaments are nested within larger scale lineaments (thin red lines within bolder lines; Fig. 3).

The flow can be subdivided into sections based on flow morphology, such as changes in the trend of prominent lineaments, topographic changes identified in GeoEye-1 imagery and flank observations (Figs. 2, 3 and 4). Two flow front lobes have been identified from GeoEye-1 imagery. The eastern lobe extends continuously from the vent, and the western lobe branches to the north (Fig. 3). Most of the prominent lineaments in the eastern lobe trend SW-NE, while smaller curvilinear features verge north eastwards. Conversely, in the western lobe, lineaments and curvilinear structures verge northwards, and the flow extends to the north. Topographic contours indicate that the western lobe responded to a change in topography, with a central flow valley dividing the lobes and topographic contours dipping NNW on the western side of the valley. Mid-flow, the Rocche Rosse sits on a continuous, steep (16–25°) topography compared to flatter (0–12°) flow front and vent regions (Fig. 2). Lineaments are continuous in mid-flow regions, before spreading radially outwards at the NE flow front. Stacks of flow ramps (Cas and Wright 1987; Gottsmann and Dingwell 2001) are evident in flank exposures in the vent region and at the break in slope of the flow front, with lava stacking up towards the mid-flow. Large-scale folding (Fig. 5) is also evident in flank exposures of the flow front.

Flow foliations

The arrangement of spherulites, microlites and vesicles defines the foliation in the obsidian lithofacies of the flow (Clay et al. 2013; Bullock et al. 2017), making it possible to recognise and measure planar structures (Figs. 5, 6 and 7; Table 1, Electronic supplementary material 1). Flow foliations are generally continuous across several metres, although they may be truncated or disrupted by small brittle faults that have a few centimetres of displacement (Clay et al. 2013). Throughout the flow, foliations are disrupted by flow-wide conjugate fracturing and tension

gashes, both up to 10 cm in length. Overall, planar structural data are randomly distributed, as evidenced by high variability of strike and dip measurements (Figs. 6 and 7). Flow foliation dips vary across flow from near vertical to horizontal, though predominance of a weak degree of preferred orientation (40%) indicates overall steeply dipping (80°) foliations towards the vent (Table 1). There is also evidence for dips preferred in a north easterly direction, away from the vent region (Fig. 7). Flow foliations dip steeply from vent towards the NE flow front (81–85°) and dip more gently towards the NW flow front (68°). The western lobe shows a moderate degree (55%) of preferred orientation (Table 1 and Fig. 7). The strike orientations and dip magnitudes vary significantly at the flow fronts, from 12 to 14° in localised areas, but more commonly > 60°. In mid-flow and near-vent regions, foliations typically dip at 30–50°, locally dipping as gently as 2–4°. There are more uniform steeply dipping mid-flow foliations in a SW-NE orientation (Fig. 7), coinciding with the positions of lineaments identified in GeoEye-1 imagery (Fig. 8). At the NE flow front, the ramping foliation typically dips 60–70° south-westerly towards the vent. At the NW flow front, ramping foliations dip from near-horizontal (16°SW) up to near-vertical (84°SW) over a few metres.

Folding

Multi-scale folds are widespread across the entire lava flow, on a scale of decimetres to tens of metres (Fig. 5). Fold asymmetry increases towards the flow fronts, with an increase in inclined axial planes (Fig. 5a–d). Sheath folding is also evident at the flow fronts (Fig. 5e–g). In particular, there are numerous folds at the NE flow front (Table 1). Small- and medium-scale flow folding (< 0.2 and 0.2–2 m wavelength and amplitude, respectively) is extensive, while larger scale folding (2–15 m wavelength and amplitude, accompanied by parasitic folds) is concentrated at the flow fronts. Up to three generations of folds have been identified, with smaller scale folds superimposed upon medium folds, and medium folds superimposed on larger folds (Fig. 5a, c, d). This is particularly evident at the break in slope at both flow fronts. Stereoplots of fold axial planes highlight an apparently random distribution of orientations and dips (Figs. 6 and 7). Density plots suggest that fold axial planes dip steeply (mean 33–60°), with the exception of horizontal trends in the vent region (mean 1°). Rose diagrams show that mid-flow fold axial planes generally dip to the NE, while folds in the vent region dip N-S (Fig. 7). Stereoplots of fold hinges highlight a range of attitudes, but the density plots (Fig. 7) show a high concentration of plunges above 60°. Fold hinges trend SE-NW, plunging 85° to 120° at a strong degree of preferred orientation of 71%, perpendicular to the prominent mid-flow lineaments identified in the GeoEye-1 image.
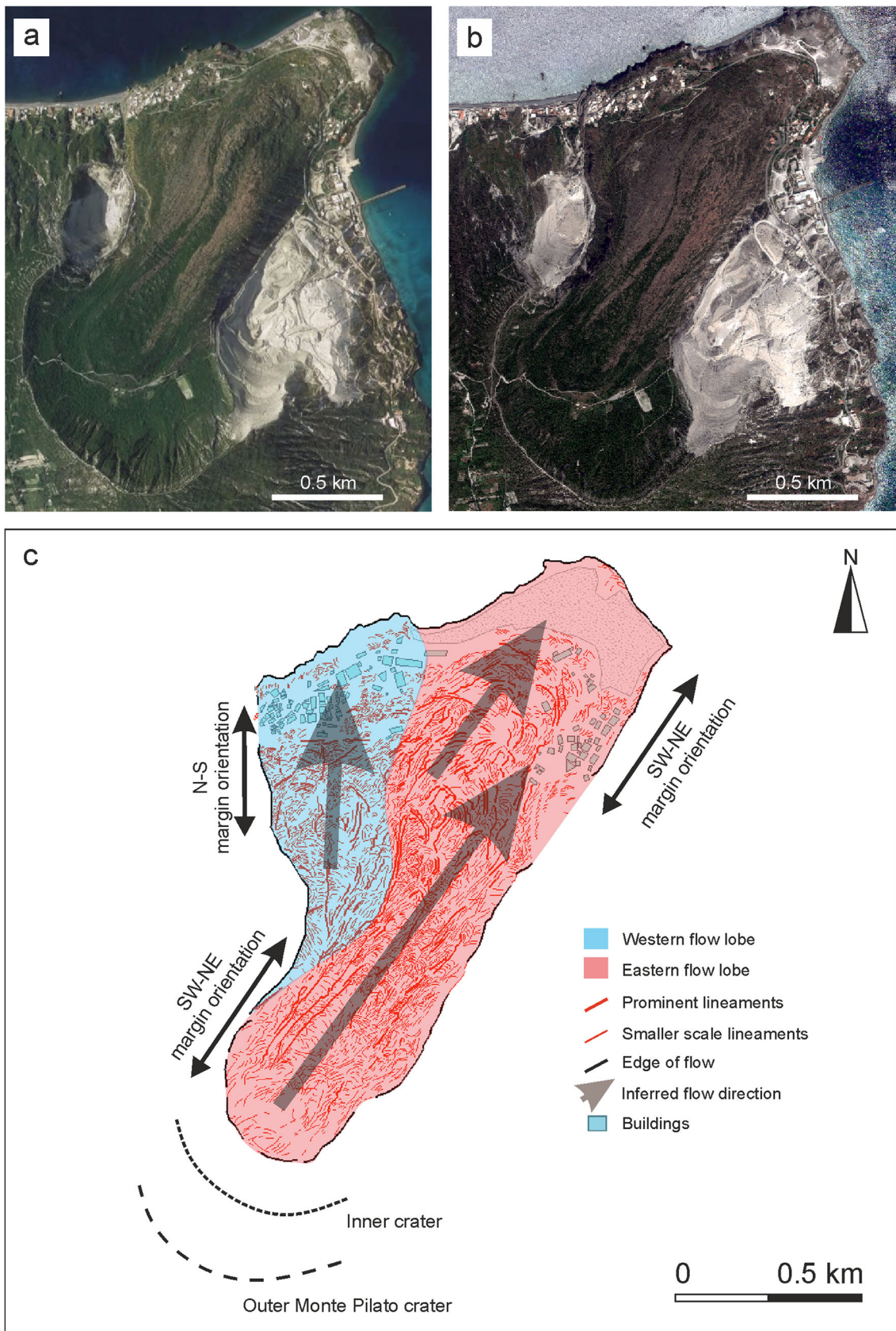
Fig. 3 a Google Earth image (Map data: SOI, NOAA, U.S. Navy, NGA, GEBCO, TerraMetrics, ©2018 Google) and **b** GeoEye-1 image of the Rocche Rosse rhyolitic lava flow. **c** Annotations of the Rocche Rosse lava flow from the satellite image, with the Monte Pilato crater vent region (dashed lines), flow margins, prominent lineaments, curvilinear features and flow lobes

c: NE flow front -
Flatter topography (10-12°)
Lineaments trending SW-NE
Curvilinear structures verging NE

a: Rocche Rosse lava flow
(entire flow extent)

b: NW flow front -
Flatter topography (0-10°)
Lineaments trending S-N
Curvilinear structures verging N

Contours

N

0   0.5 km

d: Mid-flow -
steeper topography (16-25°)
Lineaments trending SW-NE
Curvilinear structures verging NE

Key

NE flow front
NW flow front
Mid-flow
Vent region
Prominent linear and curvilinear features
Flow edge

e: Vent region - shallow topography (8-12°)
Lineaments trending SW-NE
Curvilinear structures verging NE

Fig. 4 Flow divisions based on changes in underlying slope (see contours inset and Fig. 3) and orientation/vergence of prominent lineaments and curvilinear features

Lineations

Stretching lineations, formed by shearing and resultant alignment of heterogeneities in the flow, are commonly observed mid-flow (Figs. 5 and 8), forming a parallel alignment of elongate spherulites (Bullock et al. 2017). The plunge of the stretching lineations varies from near-horizontal (2°) to vertical, with most near vertical (86° to the NE), roughly parallel to mid-flow prominent lineaments (Table 1). The majority of stretching lineations plunge steeply, with sporadic examples of near-horizontal plunges at the NW flow front and mid-flow. Mid-flow, the stretching lineations plunge more shallowly, commonly less than 30°, and in some instances, plunge back towards

the vent region, orientated NE-SW. Stretching lineations are evident in flow front regions, with more dispersed orientations. These plunges are more variable in flow front regions, but typically plunge ~ 30–40°. The NW flow front exclusively hosts steeply plunging stretching lineations.

Discussion

Crust formation

Silicate liquids of rhyolitic composition exhibit Bingham-like (non-Newtonian) rheologies below liquidus temperatures, with a non-linear dependence of strain rate on applied stress

Fig. 5 Structural features of the Rocche Rosse lava flow. **a** Small-scale (parasitic) folds (< 0.2 m wavelength and amplitude) superimposed upon medium-scale folds (0.2–2 m wavelength and amplitude) near NE flow front (*f.a.p* fold axial plane, connecting the hinge lines of the folds as a planar surface). **b** Recumbent medium-scale folding near NE flow front. **c** Large-scale (> 2 m wavelength and amplitude), inclined mid-flow folding, with medium- and small-scale parasitic folds. **d** Large-scale, recumbent fold near NW flow front (GPS for scale). **e–g** Examples of sheath folding, identified by characteristic eye shape. **h** Fractured obsidian lava. **i**, **j** Stretching lineations in mid-flow regions
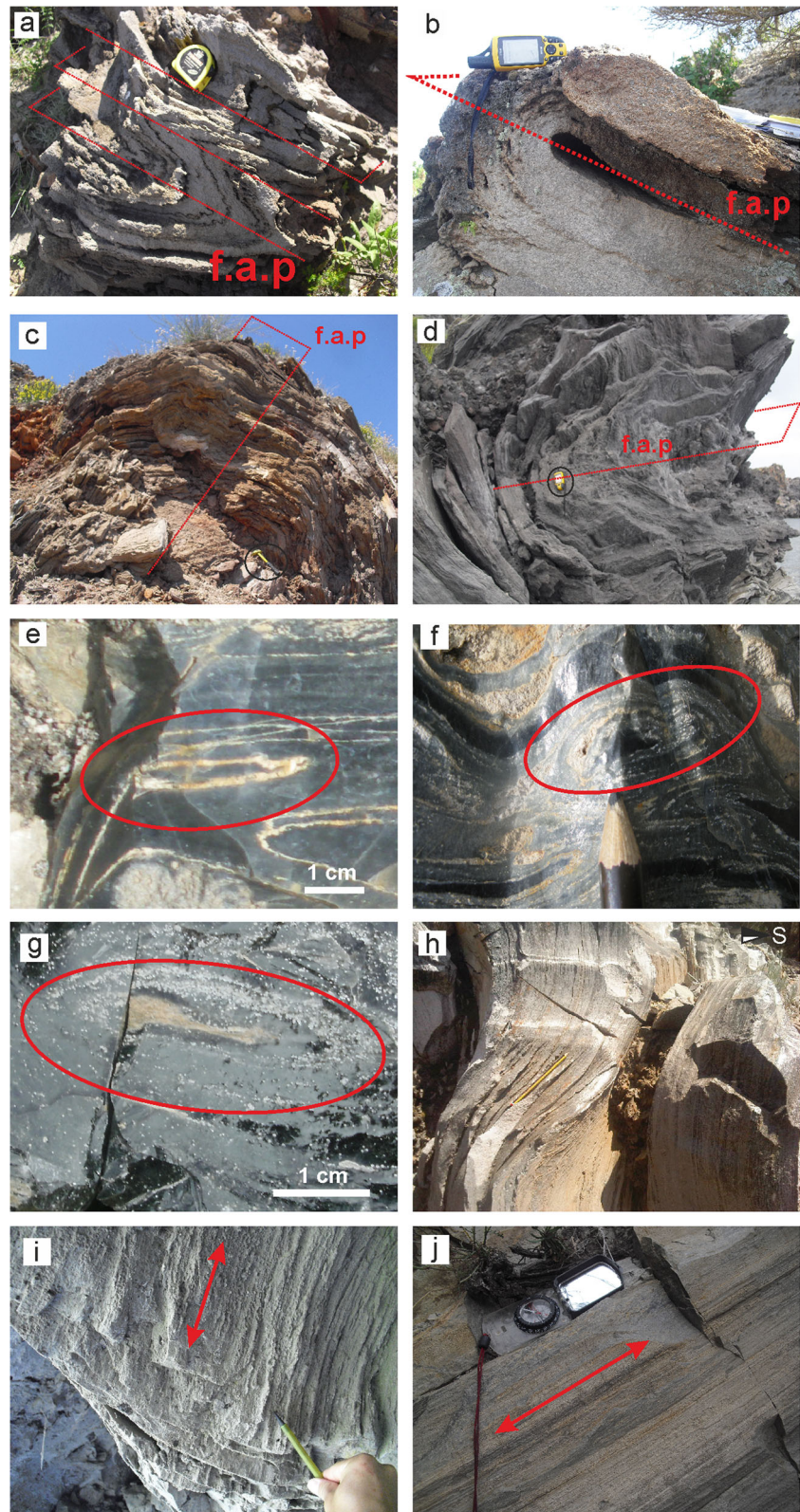
(e.g. Shaw et al. 1968; Walker 1971; Fink 1983; Webb and Dingwell 1990; Dragoni et al. 1992; Manley 1992; Fink and Griffiths 1998; Manga et al. 1998; Castro and Cashman 1999; Gottsmann and Dingwell 2001; Hess et al. 2008; Castro et al. 2013). It has been previously reported that the Rocche Rosse behaved as a Bingham fluid during emplacement (Clay et al.
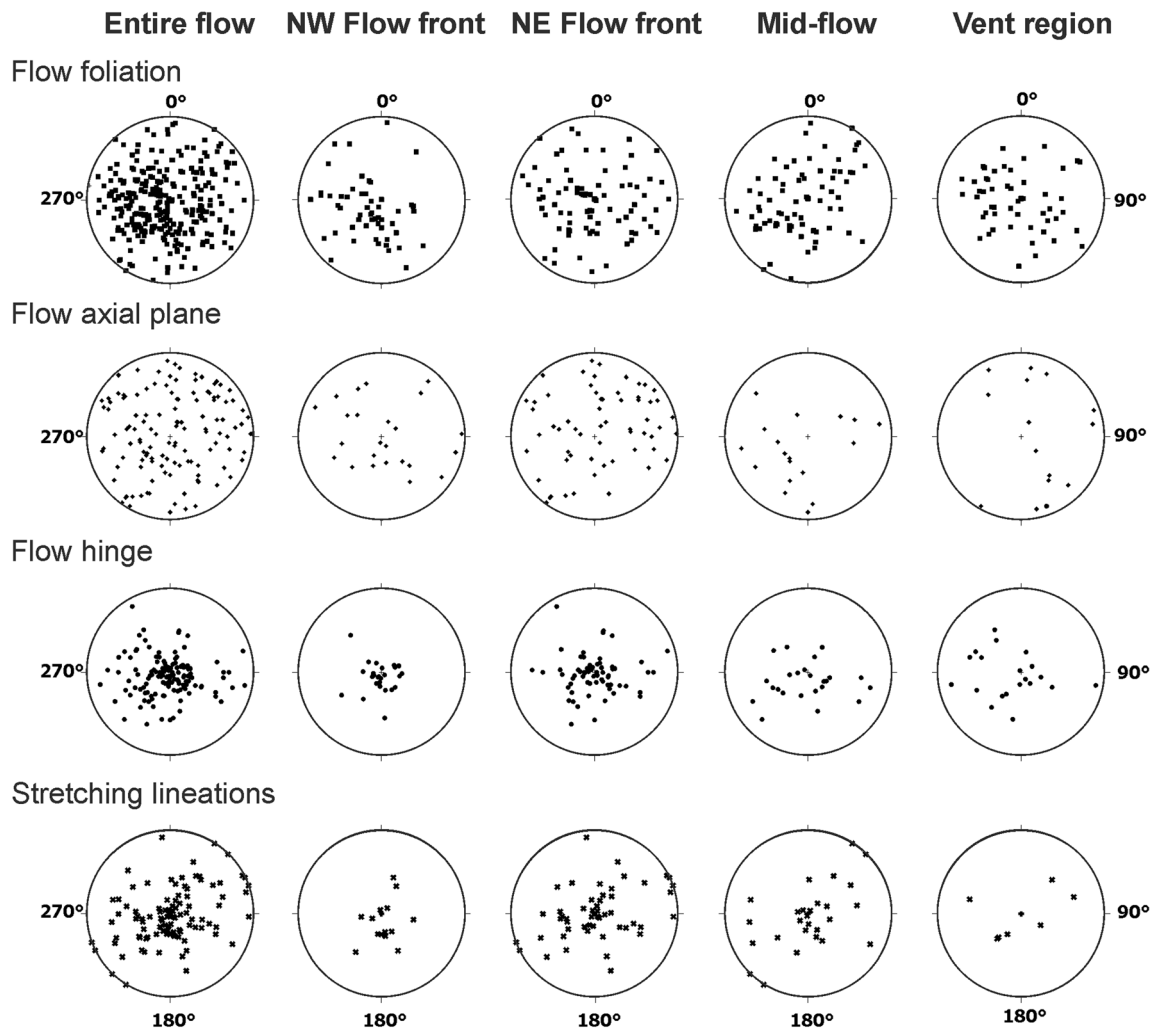
Fig. 6 Stereographic plots of flow foliations, fold axial planes, fold hinges and stretching lineations (equal area projection, lower hemisphere). Data divided into **a** entire flow, **b** NW flow front, **c** NE flow front, **d** mid flow and **e** vent region (see Fig. 4)

2013), which can promote strain localisation and folding. Strain localisation affects the rheological behaviour of lavas, and rheological contrasts between layers, such as differences in viscosity, capillary number and yield strength (Castro and Cashman 1999; Gonnerman and Manga 2005; Shields et al. 2016), can promote shear zonation. Due to the high viscosity of flowing rhyolitic lavas, the last increments of flow-related strain are recorded in the structures that are evident in the final solidified flow (Clay et al. 2013).

The model of Giordano et al. (2008) has been used here to estimate the viscosity of the Rocche Rosse rhyolite. This model predicts the non-Arrhenian Newtonian viscosity as a function of temperature and melt composition in naturally occurring silicate melts (Giordano et al. 2008). The presence of crystals and changes in crystallinity can influence viscous flow and the rheological properties of magmas (e.g. Bagdassarov and Dingwell 1992; Smith 1996; Stevenson et al. 1996; Manga et al. 1998; Griffiths 2000; Pistone et al. 2016). However, the Rocche Rosse lava flow is generally a crystal-free glass (with some exceptions; Davì et al. 2009, 2010), thus crystal content is excluded from calculations. The amount of dissolved gases, preserved as bubbles in the lava flow, can also affect viscosity and flow behaviour (e.g. Pinkerton and Sparks 1978; Lipman et al. 1985; Manga et al. 1998; Rust and Manga 2002; Llewellin and Manga 2005). However, knowledge of these influences on the apparent viscosity of a bubbly lava is limited (Stein and Spera 1992; Quane and Russell 2005; Pistone et al. 2012; Chevrel et al. 2013), and they are therefore not included in viscosity calculations here. The estimated flow surface viscosity was 10^8 to 10^{10} Pa s, using rhyolite glass chemistry from Bullock (2015); eruptive temperature range estimates (750 to 900 °C) of Cas and Wright (1987), Gottsmann and Dingwell (2001) and Davì et al. (2010); and the water content (0.08–0.25 wt%) of Shields et al. (2016). Deformation is heterogeneous and multi scale, varying greatly and non-systematically across flow (Shields et al. 2016). During emplacement, the lava probably evolved from pumiceous, through shear-banded to outgassed,
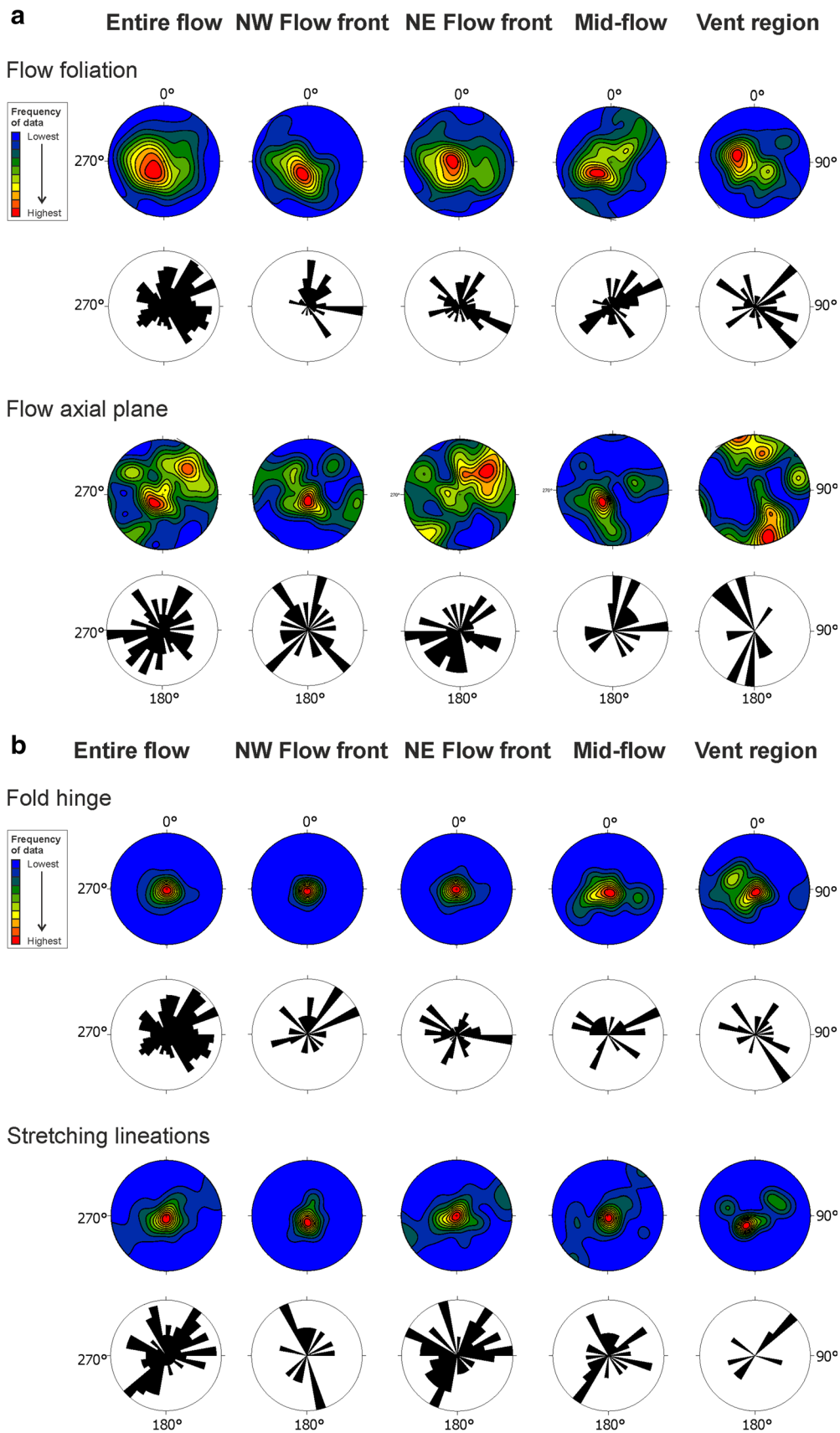
Fig. 7 Planar and linear data projected as density plots and rose diagrams (see divisions in Fig. 4). Statistical summary data available in Electronic supplementary material 2

Table 1 Summary statistics of planar and linear structural data of the Rocche Rosse lava flow (entire flow and flow segregations)

	Area of flow	Number of measurements	Mean azimuth (°)	Mean dip/plunge (°)	Mean vector (°)	Deg. of preferred orientation (%)
Entire flow						
Flow foliation	a	254	246	80	190	40
Fold axial plane	a	121	31	60	71	13
Fold hinge	a	142	208	85	120	71
Str. lineations	a	100	96	86	76	53
Flow divisions						
Flow foliation	b	52	224	68	40	55
	c	79	226	85	53	33
	d	71	257	81	49	38
	e	52	253	83	38	46
Fold axial plane	b	25	120	33	13	1
	c	61	41	51	37	21
	d	19	336	60	13	40
	e	16	358	1	11	35
Fold hinge	b	27	198	84	24	88
	c	69	177	88	60	73
	d	25	193	80	21	65
	e	21	261	70	17	61
Stretching lineations	b	15	161	81	14	83
	c	51	76	85	38	49
	d	26	85	85	20	51
	e	8	213	85	6	59

glassy obsidian (Shields et al. 2016). Vesicular magma densified through bubble collapse and fracture healing, and may have re-vesiculated to produce vesicular lava (Shields et al. 2016). As the flow continued to advance, cooling led to the development of a surface crust, which may become sufficiently strong to inhibit flow advance (Cashman et al. 1999; Blake and Bruno 2000; Hon et al. 2003; Magnall et al. 2017).

As lava flows cool, they develop a solid crust that interacts with the underlying fluid by imparting shear on the internal lava; flow advance can be inhibited as the crust strengthens (Fink and Fletcher 1978; Fink 1980a; Cashman et al. 1999; Blake and Bruno 2000; Griffiths 2000; Lescinsky and Merle 2005; Castruccio et al. 2013; Farquharson et al. 2015; Magnall et al. 2017). Rhyolitic lava crusts are typically stronger, thicker and more rigid than basaltic crusts. Holocene obsidian flows in the western US preserve evidence of a cooled surface crust in folding, crease structures and large gas cavities (Fink 1980a; Anderson and Fink 1989; Castro and Cashman 1999; Castro et al. 2002; Lescinsky and Merle 2005). Crustal development increases the strength of the flow (Hon et al. 1994; Griffiths and Fink 1997; Griffiths 2000; Lyman et al. 2005), insulates the flow and reduces heat loss (Swanson 1973; Fink and Griffiths 1998; Keszthelyi and Self 1998; Harris and Rowland 2009; Tuffen et al. 2013). When the crust fractures during lava

movement, blocky lava is formed (Finch 1933; Macdonald 1953; Fink 1980a; Harris et al. 2017), defined as being made up on distinct blocks without some of the key characteristics of an 'a'a flow, such as a spiny or clinker surface (Finch 1933).

We propose that the Rocche Rosse, with the surface characterised by blocky lava, folding, ramp structures and an overridden (basal) breccia, also was dominated by a surface crust. Early development of a surface crust is suggested by folding at the flow front and in the vent region (up to 5 m in wavelength and amplitude), formed in response to flow stagnation and buckling. Following Gregg and Fink (2000), the shallow slope underlying the Rocche Rosse vent (Fig. 2) may have aided crust formation. The surface crusts may have been strong enough to prevent breakout formation, if the internal pressure was less than the crustal yield strength (Magnall et al. 2017). Uniformly dipping SW-NE orientated foliations in mid-flow regions, where the flow is up to 50 m thick and is therefore likely to require more energy to deform, were formed by 16–25° slope-aided advance and less crustal control. Where cooling did not greatly hinder flow advance, extensional forces were promoted, evident by uniform stretching lineations in mid-flow regions (51% degree of preferred orientation; Table 1 and Fig. 8), forming perpendicular to the principle plane of shortening.

Fig. 8 Linear flow channel ridges mid-flow. **a** Interpretation of GeoEye-1 image with traced flow channels and radial spreading beyond channel. **b** Original GeoEye-1 image. **c** Structural measurements of stretching lineations in mid-flow region, the majority of measurements trending approximately NE-SW (flow direction)
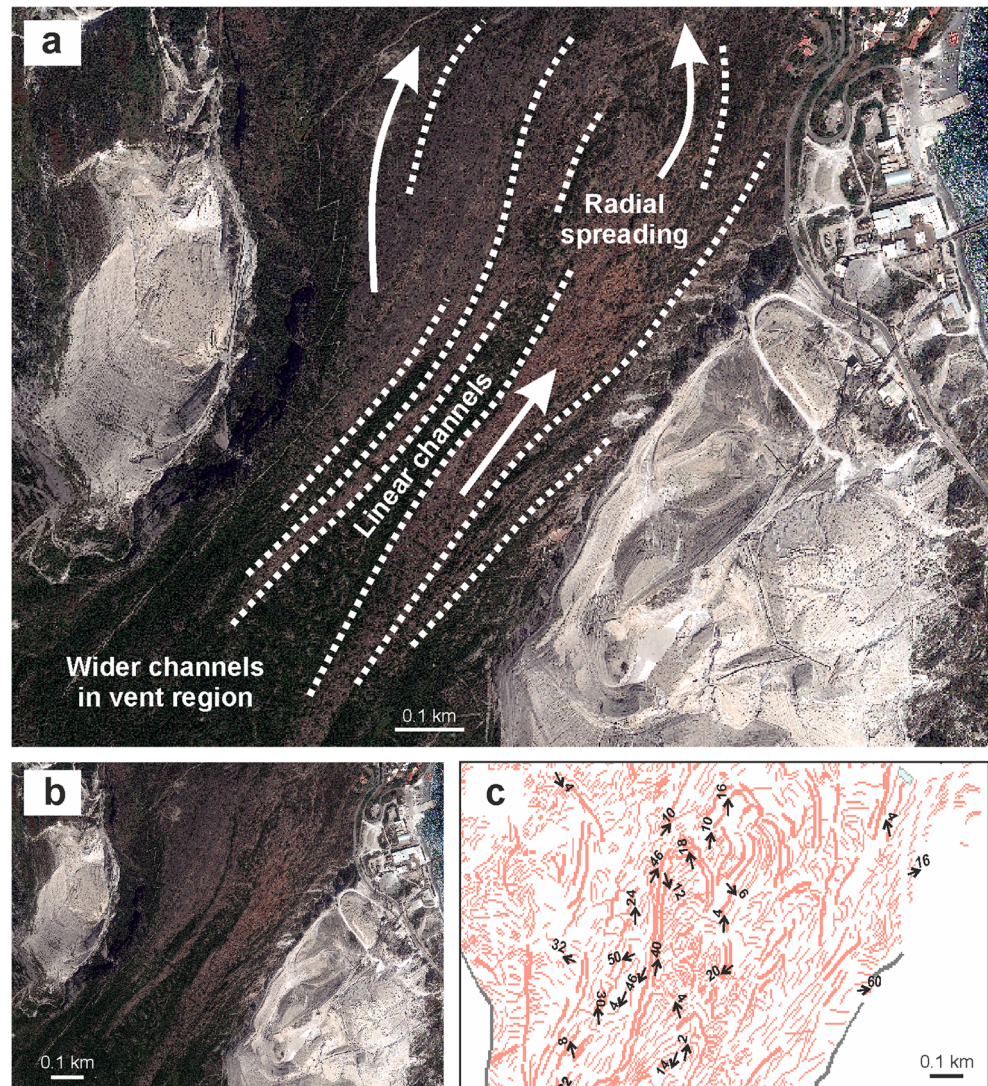
Channel development

GeoEye-1 imagery reveals a channelled flow geometry in mid-flow regions of the Rocche Rosse, with both lineaments and stretching lineations often trending parallel to flow direction (Fig. 8). This changes to lateral spreading (radial expansion) and more sporadic stretching lineation attitudes at the flow front (Fig. 8). Stretching lineations on linear ridges formed due to strike-slip shear. Similar features have been identified in other rhyolitic lava flows (Fink 1980b; Tuffen et al. 2013), and in analogue modelling of silicic lava extrusions (Fink and Griffiths 1998; Merle 1998; Gregg and Fink 2000; Griffiths 2000). During flow in a channelled regime, simple shearing is limited to the edges of the channel (Borgia et al. 1983; Dragoni et al. 1986, 1992; Harris et al. 2002). As a result, curvilinear ridges connect the stalled channel margins to the mobile central flow zone, also observed in other preserved flows (Fink 1980b; Lipman and Banks 1987; Favalli et al. 2018). Large-scale structures, including folds (height and width > 2 m), ramp structures and flow channels control local deformation, with channels hosting stretching lineations and smaller scale folds. Lateral friction along margins generated a wrenching component which, together with a viscosity contrast, can induce folding at the flow margins (Fink and Fletcher 1978). Compressional stress concentration is also promoted by deceleration of the flow front. Stretching lineations change from parallel to concentric where lateral spreading causes flow divergence (consistent with experiments of Merle 1998; Fig. 8). Channels are not evident near the vent, at the flows or in the western flow lobe, all of which lie on lower slopes. This suggests that the steeper slope produced the channelled morphology, contributing to greater stress on the surface crust, more deformational structures and a thicker flow in this area, caused by the formation of flow ramps. Thicker flow configuration mid-flow and in near-vent regions is the product of cooling-limited flow and flow build-up with continual extrusion.

Role of slope

Structural development of the Rocche Rosse relates to the underlying slope, with associated complexity of structural trends attributed to changes in slope angle and uniformity (Fig. 3). Foliations locally dip as shallow as 2–4° in near-vent regions, coinciding with a shallow slope, dipping 30–50° mid-flow over steeper topography (Figs. 6 and 7). At the NE flow front, the ramping foliation typically dips 60–70° back towards the vent (Figs. 6 and 7), suggesting crustal control and compression over a shallow topography. The variable underlying slope angle also created multi-size folds, with compression at breaks in slope superimposing earlier-formed smaller scale folds upon larger folds (Fig. 5). Analogue experiments show that the increasing extrusion rate and slope angle forms rifted, folded and leveed flows that solidified at the margins only (Gregg and Fink 2000). However, analogue experiment material behaviour may vary differently to rhyolite, and real-time rhyolite flow observations give a better indication of lobe development. Long prominent flow lobes at Cordón Caulle also form by overtopping a topographic barrier and flowing down a steepening slope (Tuffen et al. 2013). We suggest that similar processes may have been responsible for the development of the prominent western lobe in the Rocche Rosse.

On the neighbouring island of Vulcano (Fig. 1), the compositionally similar Pietre Cotte rhyolite lava flow was emplaced on a steep underlying slope of 30–35° (Frazzetta et al. 1984). The flow is characterised by a single lobe with a uniform structural arrangement of foliations and lineations, which are the result of a single flow direction over a continuous topography (Bullock 2015). Observations from the Porri andesitic lava flow on the neighbouring island of Salina (Fig. 1) indicate a steep (10–30°), uniform slope with no abrupt changes (Iezzi and Ventura 2000; Ventura 2001). Structural observations of the Porri flow indicate a decrease in fold axial plane dip away from the vent due to increasing contribution of simple shear to bulk deformation, with gravity-driven mechanisms controlling the deformation patterns (Iezzi and Ventura 2000). These observations highlight the relation between simple structural arrangement and a uniform topography. At Little Glass Mountain, CA, extension and breakout lobes from flow margins coincide with a slope increase of ~9° (Fink 1978), suggesting that a change in slope angle to this degree promotes structural complexity.

Progressive deformation

Structural complexity of the Rocche Rosse suggests that the flow underwent a sequential deformational history (Fig. 9). Fold asymmetry increases away from the vent, with more folds at flow fronts, evidence for progressive deformation (Flinn 1962; Ramsay 1979). Additional evidence for sequential deformation includes small-scale structures superimposed upon large-scale structures (Fig. 5), brittle structures cross-cutting ductile structures and the variable distribution of planar and linear orientations (Figs. 6 and 7). Progressive shear modified early-formed folds, producing sheath folds (Farrell 1984; Smith 2002; Branney et al. 2004; Andrews and Branney 2011). The time period in which the Rocche Rosse progressively deformed was likely to be weeks following effusion (Gottsmann and Dingwell 2001), and it has been suggested that deformation in rhyolitic lava flows can span a year (Lu et al. 2004; Tuffen et al. 2013).

The identification and measurement of multi-scale structures across the Rocche Rosse allows us to reconstruct emplacement and deformation mechanisms (Fig. 9). Initially, lava extruded from the Monte Pilato vent and advanced downslope towards the NE (stage 1). The first phase of compressed folding produced small-scale folds, now evident occurrence as parasitic folds on larger scale folds at the flow front (Fig. 5a–d). With advance over a steeper slope, the flow developed a channelled morphology and stretching lineations (Fig. 8; stage 2). As the topography shallowed in more distal flow regions (Fig. 2), the flow spread and compressional forces became prevalent, producing larger folds (Fig. 5a, c, d; stage 3). Cooling of the upper surface, coupled with increased strain from flow advance over a variable topography, promoted the onset of autobrecciation, which the advancing flow overrode to form the top and basal breccia. With continued extrusion, previously formed structures were reoriented by progressive deformation (stage 4), resulting in a complex arrangement of structures. For instance, the sheath folds (Fig. 5e–g) likely formed due to stretching and amplification of pre-existing curvilinear folds and structures (Reber et al. 2013). As the lava continued to advance downslope, individual flow units advanced and overlapped, forming flow ramps (Cas and Wright 1987; Gottsmann and Dingwell 2001). Continual extrusion, repetitive cycles of breaking, flowing and healing (Tuffen et al. 2003; Tuffen and Dingwell 2005; Vasseur et al. 2013; Cabrera et al. 2015) and progressive deformation produced a third generation of largest scale folding. Small-scale folds were superimposed upon the younger medium- to large-scale folding (Fig. 5a, c, d). As the lava flow cooled during emplacement, the flow probably advanced more slowly due to talus and breccia development, as well as compression against a stalled flow front (Griffiths and Fink 1992). With variations in strain rate and eventual cooling below the glass transition, more areas of the flow deformed in a brittle manner (stage 5), resulting in faults, fracturing and autobrecciation. Once the flow had cooled sufficiently, a brittle deformational phase dominated, and the flow no longer behaved as a viscous or ductile flow.
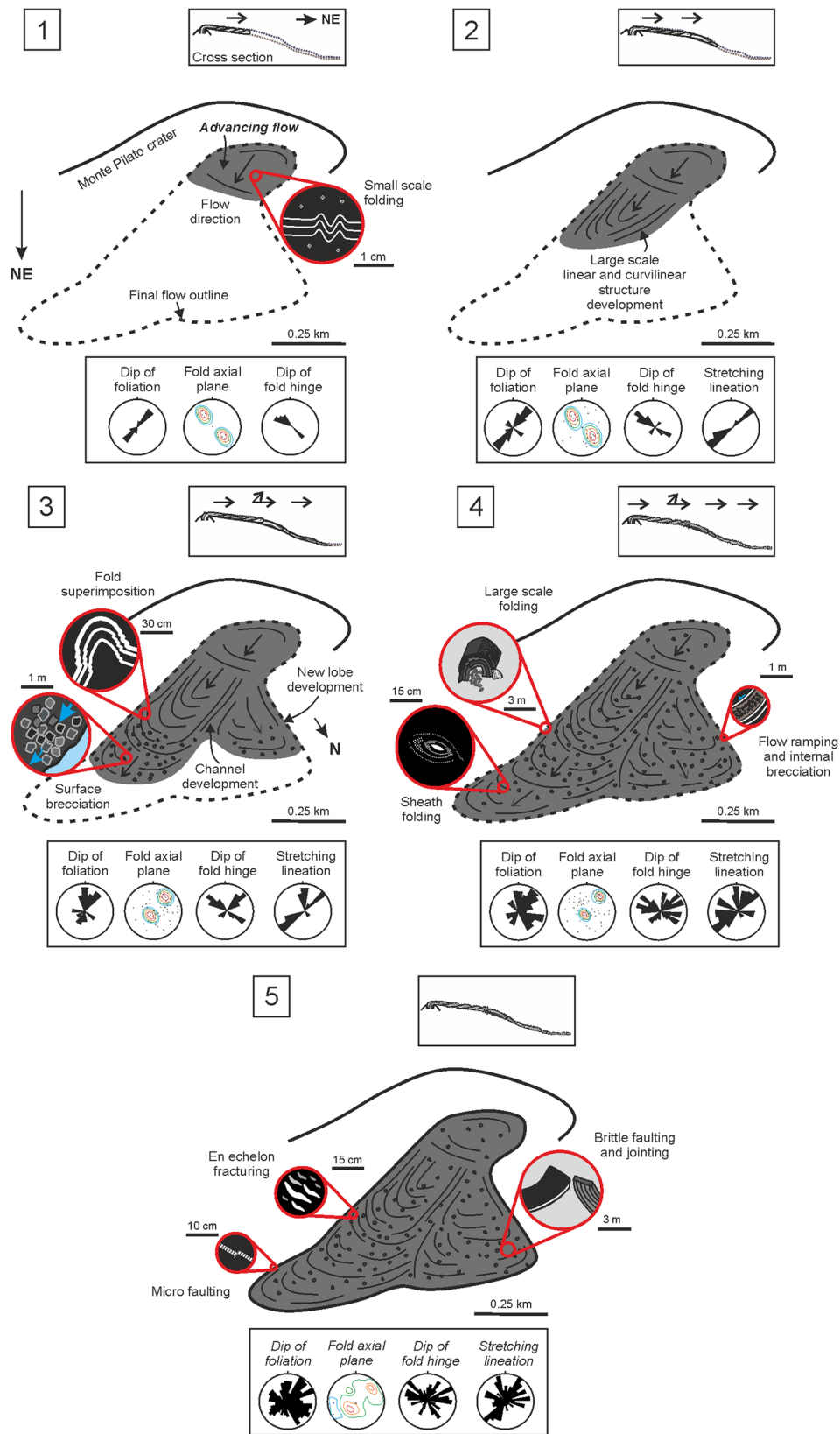
Fig. 9 Model for the emplacement of the Rocche Rosse lava flow, emplaced sequentially over five stages: (1) Initial extrusion (moving NE), crustal development and small-scale folding. (2) Extensional strain, stretching lineations and channel development over steeper topography. (3) Compression at topographic break, autobrecciation, lobe development and further (medium scale) folding. (4) Progressive deformation due to stagnation and continual extrusion, large-scale folding and re-folding. (5) Brittle deformation following flow termination. Typical structural signature associated with each stage also shown

Implications for emplacement processes

Since 2008, new observations at Chaitén and Cordón Caulle have provided an opportunity to witness emplacement of rhyolitic lava flows (Carn et al. 2009; Lara 2009; Castro et al. 2013; Schipper et al. 2013; Tuffen et al. 2013). Recent active observations also give new perspectives on the formation of older rhyolitic lavas, such as the Rocche Rosse. This is particularly true of the Cordón Caulle eruption, which flowed away from the vent (Tuffen et al. 2013), as opposed to the dome-forming eruption of Chaitén (Carn et al. 2009; Lara 2009).

Direct comparisons of structures can be made between the Rocche Rosse and Cordón Caulle obsidian flows. First, a prominent flow lobe formed at Cordón Caulle due to overtopping a topographic barrier and flow down a steepening slope (Tuffen et al. 2013; Magnall et al. 2017). We suggest the same origin for the prominent western lobe in the Rocche Rosse. The Cordón Caulle flow developed due to thermal insulation promoting flow advance, the underlying slope creating channel and compound flow formation, and the roles of a crust in controlling flow configuration and brittle domination as flow cooled (Tuffen et al. 2013; Magnall et al. 2017). These processes are all inferred in the Rocche Rosse based on observations made at Cordón Caulle, and the role played by these variable factors may be understated in the reconstruction of other older lava flows. Recent studies (Carn et al. 2009; Lara 2009; Castro et al. 2013; Schipper et al. 2013; Tuffen et al. 2013; Bertin et al. 2015; Farquharson et al. 2015; Magnall et al. 2017) of active flows and domes also highlight processes which may not be evident in older flows due to overprinting or lack of exposure.

Conclusions

The structurally complex Rocche Rosse rhyolitic lava flow preserves evidence for multi-phase emplacement and deformation stages. Due to the high viscosity of the advancing lava, indicators of emplacement processes and flow-related strain are recorded in the preserved structures of the final solidified flow. The Rocche Rosse is characterised by a channelled, compound lava flow morphology, made up of two main flow frontal lobes small (< 0.2 m) to large scale (> 2 m) folds, foliations and stretching lineations. These planar and linear structures trend and dip/plunge at highly variable orientations and magnitudes. Based on GeoEye-1 and surface observations and measurements, five concomitant stages of emplacement have been identified: (1) initial extrusion, (2) extensional strain onset, (3) compressional forces at topographic break, (4) progressive deformation and (5) a brittle deformational regime. By traditional structural measurement techniques on ancient flows and new observations made on active flows, the roles of down-flow varying dynamic processes and their role

in the overall configuration development of this flow and other older rhyolitic lava flows can be defined. For instance, the role of cooling and crust formation are important in the development of multi-scale folds, flow ramps and autobrecciation and thermal insulation and underlying slope can prolong flow propagation and promote prominent lobe formation. The structural complexity observed in the Rocche Rosse flow can be likened to the witnessed actively deforming Cordón Caulle flow, thus providing a structural framework for the evaluation of flow process emplacement interpretations.

References

Anderson SW, Fink JH (1989) Hydrogen isotope evidence for extrusion mechanisms of the Mount St. Helens dome. Nature 341:521–523

Anderson SW, Fink JH (1992) Crease structures as indicators of emplacement rates and surface stress regimes of lava flows. Geol Soc Am Bull 104:615–626

Andrews GDM, Branney MJ (2011) Emplacement and rheomorphic deformation of a large, lava-like rhyolitic ignimbrite: Grey's landing, southern Idaho. Geol Soc Am Bull 123:725–743

Arrighi S, Tanguy J, Rosi M (2006) Eruptions of the last 2200 years at Vulcano and Vulcanello (Aeolian Islands, Italy) dated by high-accuracy archaeomagnetic. Phys Earth Planet Inter 159:225–233

Bagdassarov NS, Dingwell DB (1992) A rheological investigation of vesicular rhyolite. J Volcanol Geotherm Res 50:307–322

Barberi F, Gandino A, Gioncada A, La Torre P, Sbrana A, Zenucchini C (1994) The deep structure of the Eolian arc (Filicudi-Panarea-Vulcano sector) in light of gravity, magnetic and volcanological data. J Volcanol Geotherm Res 61:189–206

Bernstein M, Pavez A, Varley N, Whelley P, Calder E (2013) Rhyolite lava dome growth styles at Chaitén volcano, Chile (2008-2009): interpretation of thermal imagery. Andean Geol 40(2):295–309

Bertin D, Lara LE, Basualto D, Amigo Á, Cardona C, Franco L, Gil F, Lazo J (2015) High effusion rates of the Cordón Caulle 2011–2012 eruption (southern Andes) and their relation with the quasi-harmonic tremor. Geophys Res Lett 42:7054–7063

Blake S, Bruno BC (2000) Modelling the emplacement of compound lava flows. Earth Planet Sci Lett 184:181-197

Borgia A, Linneman S, Spencer D, Morales LD, Andre JB (1983) Dynamics of lava flow fronts, Arenal volcano, Costa Rica. J Volcanol Geotherm Res 19:303–329

Branney MJ, Barry TL, Godchaux M (2004) Sheathfolds in rheomorphic ignimbrites. Bull Volcanol 66:485–491

Breitkreuz C (2013) Spherulites and lithophysae—200 years of investigation on high-temperature crystallization domains in silica-rich volcanic rocks. Bull Volcanol 75:1–16

Bullock LA (2015) Structure, emplacement and textural evolution of young obsidian lavas in the Aeolian Islands, Italy. PhD thesis, Keele University, UK

Bullock LA, Gertisser R, O'Driscoll B (2017) Spherulite formation in obsidian lavas in the Aeolian Islands, Italy. Period Mineral 86:37–54

Cabrera A, Weinberg R, Wright HM (2015) Magma fracturing associated with obsidian formation: the explosive-effusive transition. J Volcanol Geotherm Res 298:71–84

Calvari S, Pinkerton H (1999) Lava tube morphology on Etna and evidence for lava flow emplacement mechanisms. J Volcanol Geotherm Res 90:263–280

Carn SA, Pallister JS, Lara L, Ewert JW, Watt S, Prata AJ, Thomas RJ, Villarosa G (2009) The unexpected awakening of Chaitén volcano, Chile. EOS Trans Am Geophys Union 90(24):205–206

Cas RAF, Wright JV (1987) Volcanic successions. Modern and ancient. Allen and Unwin, London, p 528

Cashman KV, Kauahikaua JP, Thornber C (1999) Cooling and crystallization of lava in open channels, and the transition of pahoehoe lava to 'a'ā. Bull Volcanol 61:306–323

Castro JM, Cashman KV (1999) Constraints on rheology of obsidian and pumice based on folds in obsidian lavas. J Struct Geol 21:807–819

Castro JM, Manga M, Cashman K (2002) Dynamics of obsidian flows inferred from microstructures: insights from microlite preferred orientations. Earth Planet Sci Lett 199(1–2):211–226

Castro JM, Beck P, Tuffen H, Nichols ARL, Martin M (2008) Timescales of spherulite crystallization in obsidian inferred from water concentration profiles. Am Mineral 93:1816–1822

Castro JM, Schipper CI, Mueller S, Militzer A, Amigo A, Parejas CS, Jacob D (2013) Storage and eruption of near-liquidus rhyolite magma at Cordón Caulle, Chile. Bull Volcanol 75:702–719

Castro JM, Bindeman IN, Tuffen H, Schipper IC (2014) Explosive origin of silicic lava: textural and H_2O evidence for pyroclastic degassing during rhyolite effusion. Earth Planet Sci Lett 405:52–61

Castruccio A, Rust A, Sparks R (2013) Evolution of crust- and core-dominated lava flows using scaling analysis. Bull Volcanol 75(1):1–15

Chevrel MO, Platz T, Hauber E, Baratoux D, Lavallee Y, Dingwell DB (2013) Lava flow rheology: a comparison of morphological and petrological methods. Earth Planet Sci Lett 384:109–120

Cioni R, Funedda A (2005) Structural geology of crystal-rich, silicic flows: a case study from San Pietro Island (Sardinia, Italy). Geol Soc Am 396:1–14

Clay PL, O'Driscoll B, Gertisser R, Busemann H, Sherlock SC, Kelley SP (2013) Textural characterization, major and volatile element quantification and Ar–Ar systematics of spherulites in the Rocche Rosse obsidian flow, Lipari, Aeolian Islands: a temperature continuum growth model. Contrib Mineral Petrol 165(2):373–395

Cortese M, Frazzetta G, La Volpe L (1986) Volcanic history of Lipari (Aeolian Islands, Italy) during the last 10,000 years. J Volcanol Geotherm Res 27(1–2):117–133

Davì M, De Rosa R, Barca D (2009) A LA-ICP-MS study of minerals in the Rocche Rosse magmatic enclaves: evidence of a mafic input triggering the latest silicic eruption of Lipari Island (Aeolian Arc, Italy). J Volcanol Geotherm Res 182:45–56

Davì M, De Rosa R, Holtz F (2010) Mafic enclaves in the rhyolitic products of Lipari historical eruptions; relationships with the coeval Vulcano magmas (Aeolian Islands, Italy). Bull Volcanol 72:991–1008

de Silva SL, Self S, Francis PW, Drake RE, Carlos Ramirez R (1994) Effusive silicic volcanism in the Central Andes: the Chao dacite and other young lavas of the Altiplano-Puna volcanic complex. J Geophys Res 99(B9):17805–17825

Dellino P, La Volpe L (1995) Fragmentation versus transportation mechanism in the pyroclastic sequence of Monte Pilato-Rocche Rosse (Lipari, Italy). J Volcanol Geotherm Res 64:211–231

Dragoni M, Bonafede M, Boschi E (1986) Downslope flow model of a Bingham liquid: implications for lava flows. J Volcanol Geotherm Res 30:305–325

Dragoni M, Pondrelli S, Tallarico A (1992) Longitudinal deformation of a lava flow: the influence of Bingham rheology. J Volcanol Geotherm Res 52:247–254

Farquharson JI, James MR, Tuffen H (2015) Examining rhyolite lava flow dynamics through photo-based 3D reconstructions of the 2011–2012 lava flow field at Cordón-Caulle, Chile. J Volcanol Geotherm Res 304:336–348

Farrell SG (1984) A dislocation model applied to slump structures, Ainsa Basin, south central Pyrenees. J Struct Geol 6:727–736

Favalli M, Fornaciai A, Nannipieri L, Harris A, Calvari S, Lormand C (2018) UAV-based remote sensing surveys of lava flow fields: a case study from Etna's 1974 channel-fed lava flows. Bull Volcanol 80:29

Finetti I, Morelli C (1973) Geophysical exploration of the Mediterranean Sea. Boll Geofis Teor Appl 15:263–344

Fink JH (1978) Surface structures on obsidian flows. PhD thesis, Stanford University, USA

Fink JH (1980a) Gravity instability in the Holocene big and little Glass Mountain rhyolitic obsidian flows, northern California. Tectonophysics 66:144–166

Fink JH (1980b) Surface folding and viscosity of rhyolite flows. Geology 8:250–254

Fink JH (1983) Structure and emplacement of a rhyolitic obsidian flow: little Glass Mountain, medicine Lake highland, northern California. Geol Soc Am Bull 94:362–380

Fink JH, Fletcher RC (1978) Ropy pahoehoe: surface folding of a viscous fluid. J Volcanol Geotherm Res 4:151–170

Fink JH, Griffiths RW (1998) Morphology, eruption rates, and rheology of lava domes: insights from laboratory models. J Geophys Res 103(B1):527–545

Finch RH (1933) Block Lava. J Geol 41(7):769-770

Flinn D (1962) On folding during three-dimensional progressive deformation. Q J Geol Soc 118:385–433

Forni F, Lucchi F, Peccerillo A, Tranne CA, Rossi PL, Frezzotti ML (2013) Stratigraphy and geological evolution of the Lipari volcanic complex (central Aeolian archipelago). In: Lucchi F et al (eds) The Aeolian Islands volcanoes. Geol Soc Lond Memoirs 37:395–469

Frazzetta G, La Volpe L, Sheridan MF (1984) Evolution of the Fossa cone, Vulcano. J Volcanol Geotherm Res 17:329–360

Fujii T, Nakada S (1999) The 15 September 1991 pyroclastic flows at Unzen volcano (Japan): a flow model for associated ash-cloud surges. J Volcanol Geotherm Res 89:159–172

Gardner JE, Befus KS, Watkins J, Hesse M, Miller N (2012) Compositional gradients surrounding spherulites in obsidian and their relationship to spherulite growth and lava cooling. Bull Volcanol 74(8):1865–1879

Gioncada A, Mazzuoli R, Bisson M, Pareschi MT (2003) Petrology of volcanic products younger than 42 ka on the Lipari-Vulcano complex (Aeolian Islands, Italy): an example of volcanism controlled by tectonics. J Volcanol Geotherm Res 122(3–4):191–220

Gioncada A, Mazzuoli R, Milton AJ (2005) Magma mixing at Lipari (Aeolian Islands, Italy): insights from textural and compositional features of phenocrysts. J Volcanol Geotherm Res 145(1–2):97–118

Giordano D, Russell JK, Dingwell DB (2008) Viscosity of magmatic liquids: a model. Earth Planet Sci Lett 271:123–134

Gonnermann HM, Manga M (2003) Flow banding in obsidian: a record of evolving textural heterogeneity during magma deformation. Earth Planet Sci Lett 236:135–147

Gonnermann H, MANGA M, (2005) Nonequilibrium magma degassing: Results from modeling of the ca. 1340 A.D. eruption of Mono Craters, California. Earth Planet Sci Lett 238(1-2):1–16

Gottsmann J, Dingwell DB (2001) The cooling of frontal flow ramps: a calorimetric study on the Rocche Rosse rhyolite flow, Lipari, Aeolian Island, Italy. Terra Nova 13:157–164

Gregg TKP, Fink JH (2000) A laboratory investigation into the effects of slope on lava flow morphology. J Volcanol Geotherm Res 96:145–159

Griffiths RW (2000) The dynamics of lava flows. Annu Rev Fluid Mech 32:477–518

Griffiths RW, Fink JH (1992) The morphology of lava flows in planetary environments: predictions from analog experiments. J Geophys Res 97(B13):19739–19748

Griffiths RW, Fink JH (1997) Solidifying Bingham extrusions: a model for the growth of silicic lava domes. J Fluid Mech 347:13–36

Gvirtzman Z, Nur A (2001) Residual topography, lithospheric thickness, and sunken slabs in the central Mediterranean. Earth Planet Sci Lett 187:117–130

Hall SH (1978) The stratigraphy of Northern Lipari and the structure of the Rocche Rosse rhyolite lava flow and its implications. BSc thesis, University of Leeds, pp 89

Harris AJL, Rowland, SK (2009) Effusion rate controls on lava flow length and the role of heat loss: a review. In: Thordarson et al. (eds) studies in volcanology: the legacy of George Walker, spec. Publ. IAVCEI, vol. 2, Geol Soc Lon, UK, p 33–51

Harris AJL, Flynn LP, Matias O, Rose WI (2002) The thermal stealth flows of Santiaguito: implications for the cooling and emplacement of dacitic block lava flows. Geol Soc Am Bull 114(5):533–546

Harris AJL, Flynn LP, Matias O, Rose WI, Cornejo J (2004) The evolution of an active silicic lava flow field: an ETM+ perspective. J Volcanol Geotherm Res 135(1–2):147–168

Harris AJL, Rowland SK, Villeneuve N, Thordarson T (2017) Pāhoehoe, 'a'ā, and block lava: an illustrated history of the nomenclature. Bull Volcanol 79:7

Hess KU, Cordonnier B, Lavallée Y, Dingwell DB (2008) Viscous heating in rhyolite: an in situ experimental determination. Earth Planet Sci Lett 275:121–126

Hon K, Gansecki C, Kauahikaua J (2003) The transition from 'a'ā to pāhoehoe crust on flows emplaced during the Pu'u 'Ō'ō-Kūpaianaha eruption. US Geol Surv Prof Pap 1676:89–103

Hon K, Kauahikaua J, Denlinger R, McKay K (1994) Emplacement and inflation of pahoehoe sheet flows: observations and measurements of active lava flows on Kilauea volcano Hawaii. Geol Soc Am Bull 106:351–370

Iezzi G, Ventura G (2000) Kinematics of lava flows based on folds analysis. Geophys Res Lett 27(8):1227–1231

Jerram DA (2002) Volcanology and facies architecture of flood basalts. Geol Soc Am Spec Pap 362:119–132

Keszthelyi L, Self S (1998) Some physical requirements for the emplacement of long basaltic lava flows. J Geophys Res 103(B11):27447–27464

Kilburn CRJ (2000) Lava flows and flow fields. In: Sigurdsson (ed) Encyclopedia of volcanoes. Academic Press, San Diego, pp 291–305

Lara LE (2009) The 2008 eruption of the Chaitén volcano, Chile—a preliminary report. Andean Geol 36(1):125–129

Latutrie B, Harris A, Médard E, Gurioli L (2017) Eruption and emplacement dynamics of a thick trachytic lava flow of the Sancy volcano (France). Bull Volcanol 79:4. https://doi.org/10.1007/s00445-016-1084-6

Lescinsky DT, Merle O (2005) Extensional and compressional strain in lava flows and the formation of fractures in surface crust. In: Manga M, Ventura G (eds) Kinematics and dynamics of lava flows. Geol Soc Am Spec Pap 396:163–179

Lipman PW, Banks NG (1987) Aa flow dynamics. In: Decker RW, Wright TL, Stauffer PH (eds) Volcanism in Hawaii. Mauna Loa, 1984, chap. 57. US Geol Surv Prof Pap 1350 (2):1527–1567

Lipman PW, Banks NG, Rhodes JM (1985) Degassing-induced crystallization of basaltic magma and effects on lava rheology. Nature 317:604–607

Llewellin EW, Manga M (2005) Bubble suspension rheology and implications for conduit flow. J Volcanol Geotherm Res 143(1–3):205–217

Lofgren GE (1971) Spherulitic textures in glassy and crystalline rocks. J Geophys Res 76(23):5635–5648

Lu Z, Rykhus R, Masterlark T, Dean KG (2004) Mapping recent lava flows at Westdahl volcano, Alaska, using radar and optical satellite imagery. Remote Sens Environ 91:345–353

Lucchi F, Tranne CA, Rossi PL (2010) Stratigraphic approach to geological mapping of the late quaternary volcanic island of Lipari (Aeolian archipelago, southern Italy). In: Groppelli G, Goette LV (eds) Stratigraphy and geology of volcanic areas. pp 1–32

Lyman AW, Kerr RW, Griffiths RW (2005) The effects of internal rheology and surface cooling on the emplacement of lava flows. J Geophys Res 110:B08207

Macdonald GA (1953) Pahoehoe, aa, and block lava. Am J Sci 251(3):169–191

Magnall N, James MR, Tuffen H, Vye-Brown C (2016) Similarities in basalt and rhyolite lava flow emplacement processes. Geophys Res Abstr 18:9199

Magnall N, James MR, Tuffen H, Vye-Brown C (2017) Emplacing a cooling limited rhyolite flow. Volcanic and Magmatic Studies Group Annual Meeting, Liverpool, Abstr, p 141

Manga M (1998) Orientation distribution of microlites in obsidian. J Volcanol Geotherm Res 86:107–115

Manga M, Castro J, Cashman KV, Loewenberg M (1998) Rheology of bubble-bearing magmas. J Volcanol Geotherm Res 87:15–28

Manley CH (1992) Extended cooling and viscous flow of large, hot rhyolite lavas: implications of numerical modeling results. J Volcanol Geotherm Res 53:27–46

Manley CH, Fink JH (1987) Internal textures of rhyolite flows as revealed by research drilling. Geology (Boulder) 15(6):549–552

McArthur AN, Cas RAF, Orton GJ (1998) Distribution and significance of crystalline, perlitic and vesicular textures in the Ordovician Garth tuff (Wales). Bull Volcanol 60:260–285

Merle O (1998) Internal strain within lava flows from analogue modelling. J Volcanol Geotherm Res 81:189–206

Pallister JS, Diefenbach AK, Burton WC, Muñoz J, Griswold JP, Lara LE, Lowenstern JB, Valenzuela CE (2013) The Chaitén rhyolite lava dome: eruption sequence, lava dome volumes, rapid effusion rates and source of the rhyolite magma. Andean Geol 40(2):277–294

Passey S, Bell B (2007) Morphologies and emplacement mechanisms of the lava flows of the Faroe Islands basalt group, Faroe Islands, NE Atlantic ocean. Bull Volcanol 70(2):139–156

Pinkerton H, Sparks RSJ (1978) Field measurements of the rheology of lava. Nat Lett 276:382–385

Pistone M, Caricchi L, Ulmer P, Burlini L, Ardia P, Reusser E, Marone F, Arbaret L (2012) Deformation experiments of bubble- and crystal-bearing magmas: rheological and microstructural analysis. J Geophys Res 117:B05208

Pistone M, Cordonnier B, Caricchi L, Ulmer P, Marone F (2016) The viscous to brittle transition in crystal- and bubble-bearing magmas. Front. Earth Sci 3:71

Quane SL, Russell JK (2005) Welding: insights from high-temperature analogue experiments. J Volcanol Geotherm Res 142(1–2):67–87

Ramsay DM (1979) Analysis of rotation of folds during progressive deformation. Geol Soc Am Bull 98(8):732–738

Reber JE, Dabrowski M, Galland O, Schmid DW (2013) Sheath fold morphology in simple shear. J Struct Geol 53:15–26

Rust AC, Manga M (2002) Effects of bubble deformation on the viscosity of dilute suspensions. J Non-Newtonian Fluid Mech 104:53–63

Schipper CI, Castro JM, Tuffen H, James MR, How P (2013) Shallow vent architecture during hybrid explosive–effusive activity at Cordón Caulle (Chile, 2011–12): evidence from direct observations and pyroclast textures. J Volcanol Geotherm Res 262:25–37

Self S, Thordarsson T, Keszthelyi L (1997) Emplacement of continental flood basalt lava flows. In: Mahoney, Coffin (eds) Large igneous provinces: continental, oceanic, and planetary flood volcanism. AGU, Washington, D. C

Shaw HR, Wright TL, Peck DL, Okamura R (1968) The viscosity of basaltic magma: an analysis of field measurements in Makaopuhi lava Lake, Hawaii. Am J Sci 266:225–264

Shields JK, Mader HM, Caricchi L, Tuffen H, Mueller S, Pistone M, Baumgartner L (2016) Unravelling textural heterogeneity in obsidian: shear-induced outgassing in the Rocche Rosse flow. J Volcanol Geotherm Res 310:137–158

Smith JV (1996) Ductile-brittle transition structures in the basal shear zone of a rhyolite lava flow, eastern Australia. J Volcanol Geotherm Res 72:217–223

Smith JV (2002) Structural analysis of flow-related textures in lavas. Earth-Sci Rev 57(3–4):279–297

Stein DJ, Spera FJ (1992) Rheology and microstructure of magmatic emulsions: theory and experiments. J Volcanol Geotherm Res 49: 157–174

Stevenson RJ, Hodder APW, Briggs RM (1996) Rheological estimates of rhyolite lava flows from the Okataina volcanic Centre, New Zealand. N Z J Geol Geophys 37(2):211–221

Swanson DA (1973) Pahoehoe flows from the 1969-1971 Mauna Ulu eruption, Kilauea volcano, Hawaii. Geol Soc Am Bull 84:615–626

Swanson SE (1977) Relation of nucleation and crystal-growth rate to the development of granitic textures. Am Mineral 62:966–978

Tuffen H, Dingwell DB (2005) Fault textures in volcanic conduits: evidence for seismic trigger mechanisms during silicic eruptions. J Volcanol Geotherm Res 67(4):370–387

Tuffen H, Dingwell DB, Pinkerton H (2003) Repeated fracture and healing of silicic magma generate flow banding and earthquakes? Geology 31(12):1089–1092

Tuffen H, James M, Castro JM, Schipper I (2013) Exceptional mobility of an advancing rhyolitic obsidian flow at Cordón Caulle volcano in Chile. Nat Commun 4:2709

Uia T, Matsuwob N, Sumitac M, Fujinawad A (1999) Generation of block and ash flows during the 1990–1995 eruption of Unzen volcano, Japan. J Volcanol Geotherm Res 89(1–4):123–137

Vasseur J, Wadsworth FB, Lavallée Y, Hess KU, Dingwell DB (2013) Volcanic sintering: timescales of viscous densification and strength recovery. Geophys Res Lett 40:5658–5664

Ventura G (2001) The strain path and emplacement mechanism of lava flows: an example from Salina (southern Tyrrhenian Sea, Italy). Earth Planet Sci Lett 188:229–240

Ventura G (2013) Kinematics of the Aeolian volcanism (southern Tyrrhenian Sea) from geophysical and geological data. In: Lucchi F et al (eds) The Aeolian Islands volcanoes. Geol Soc Lond Memoirs 37:3–11

Walker GPL (1971) Compound and simple lava flows and flood basalts. Bull Volcanol 35(3):579–590

Webb S, Dingwell DB (1990) The onset of non-Newtonian rheology of silicate melts. Phys Chem Miner 17:125-132